

**UNIVERSIDAD SAN FRANCISCO DE QUITO USFQ**

**Colegio de Ciencias e Ingenierías**

**Subthreshold Model of the Graphene-Silicon Interface in  
Schottky Diodes**

**Katty Doménica Beltrán Cahueñas**

**Co-Autor: Jhon Jairo Paredes Mayorga**

**Ingeniería Electrónica**

Trabajo de fin de carrera presentado como requisito  
para la obtención del título de  
Ingeniera Electrónica

Quito, 14 de diciembre de 2023

**UNIVERSIDAD SAN FRANCISCO DE QUITO USFQ**

**Colegio de Ciencias e Ingenierías**

**HOJA DE CALIFICACIÓN  
DE TRABAJO DE FIN DE CARRERA**

**Subthreshold Model of the Graphene-Silicon Interface in  
Schottky Diodes**

**Katty Doménica Beltrán Cahueñas**

**Nombre del profesor, Título académico**

**Luis Miguel Prócel, PhD  
Javier Torres, PhD  
Cesar Zambrano, PhD**

Quito, 14 de diciembre de 2023

## © DERECHOS DE AUTOR

Por medio del presente documento certifico que he leído todas las Políticas y Manuales de la Universidad San Francisco de Quito USFQ, incluyendo la Política de Propiedad Intelectual USFQ, y estoy de acuerdo con su contenido, por lo que los derechos de propiedad intelectual del presente trabajo quedan sujetos a lo dispuesto en esas Políticas.

Asimismo, autorizo a la USFQ para que realice la digitalización y publicación de este trabajo en el repositorio virtual, de conformidad a lo dispuesto en la Ley Orgánica de Educación Superior del Ecuador.

Nombres y apellidos: Katty Doménica Beltrán Cahueñas

Código: 00206846

Cédula de identidad: 1726020405

Lugar y fecha: Quito, 14 de diciembre de 2023

## **ACLARACIÓN PARA PUBLICACIÓN**

**Nota:** El presente trabajo, en su totalidad o cualquiera de sus partes, no debe ser considerado como una publicación, incluso a pesar de estar disponible sin restricciones a través de un repositorio institucional. Esta declaración se alinea con las prácticas y recomendaciones presentadas por el Committee on Publication Ethics COPE descritas por Barbour et al. (2017) Discussion document on best practice for issues around theses publishing, disponible en <http://bit.ly/COPETHeses>.

## **UNPUBLISHED DOCUMENT**

**Note:** The following capstone project is available through Universidad San Francisco de Quito USFQ institutional repository. Nonetheless, this project – in whole or in part – should not be considered a publication. This statement follows the recommendations presented by the Committee on Publication Ethics COPE described by Barbour et al. (2017) Discussion document on best practice for issues around theses publishing available on <http://bit.ly/COPETHeses>.

## RESUMEN

El presente trabajo se centra en el estudio, simulación y caracterización de la interfaz grafeno-silicio. Se consideran dos enfoques principales: uno a nivel de física y otro a nivel de dispositivo. En el aspecto de la física, se realiza un análisis cuántico-mecánico mediante el software Quantum ATK para aproximar computacionalmente la ecuación de Schrödinger utilizando la Teoría del Funcional de la Densidad (DFT). A nivel de dispositivo, se lleva a cabo un análisis electrodinámico a partir de los resultados obtenidos en el nivel anterior, utilizando el software Sentaurus para resolver la ecuación de Poisson en varios puntos a lo largo de la juntura grafeno-silicio.

A través de los resultados de la simulación, se determina un modelo subumbral, y se evalúa la contribución de diferentes mecanismos de transporte de corriente, proporcionando información valiosa sobre el comportamiento del dispositivo.

**Palabras clave:** Interfaz grafeno-silicio, modelo TCAD, diodo Schottky, modelo subthreshold, DFT, Poisson, QuantumATK, Sentaurus

## ABSTRACT

The present work focuses on the study, simulation, and characterization of the graphene-silicon interface. Two main approaches are considered: one at the physics level and another at the device level. In the physics aspect, a quantum-mechanical analysis is conducted through Quantum ATK software to computationally approximate Schrodinger's equation using the Density Functional Theory (DFT). On the device level, an electrodynamic analysis is performed from the results obtained in the previous level, and Sentaurus software is used to solve the Poisson equation at various points along the graphene-Si junction.

Through the simulation results, a subthreshold model is derived, and the contribution of different current transport mechanisms is evaluated, providing valuable insights into the behavior of the device.

**Key words:** Graphene-Si interface, TCAD model, Schottky diode, subthreshold model, DFT, Poisson, QuantumATK, Sentaurus

**TABLE OF CONTENTS**

Introduction.....	10
State of the Art.....	11
Methodology.....	19
Results.....	20
Conclusions and Future Work .....	31
References.....	33
Annex A: Code 1 - sde_dvs.cmd .....	35
Annex B: Code 2 - Metal.par or Graphene Model.....	36
Annex C: Code 3 - sdevice_des.cmd .....	40
Annex D: Code 4 - sdevice_des1.cmd.....	42
Annex E: Code 5 - sdevice.par .....	44

**TABLE INDEX**

Table 1. Parameters of the crystal supercell. ....	21
Table 2. Physical Parameters of the Graphene Layer .....	23
Table 3: Comparison of Subthreshold Model parameters with Casalino's experimental curve. .....	31



## FIGURES INDEX

Figure 1. Band diagram of a metal-semiconductor junction. (a) n-type semiconductor. (b) p-type semiconductor. [7] .....	14
Figure 2. Tunneling current components. [10] .....	18
Figure 3. Formation of the graphene-Si crystal supercell.....	20
Figure 4. Graphene-Si crystal supercell - Optimized configuration.....	21
Figure 5. Band Structure of the graphene layer. (a) Optimized configuration. (b) -1 Å displacement. (c) +2.5 Å displacement.....	22
Figure 6. Graphene-Si Schottky Diode in Sentaurus, Graphene = 5nm (wide), Si = 1 μm (wide).....	24
Figure 7. IV Curves due to Thermionic Emission - Semilog scale. ....	25
Figure 8. IV Curves due to Diffusion - Semilog scale.....	27
Figure 9. IV Curves due to Tunneling - Semilog scale.....	28
Figure 10. Tunnel Effect in the Schottky diode.....	28
Figure 11. Schottky IV Curve. (a) Subthreshold Model. (b) Subthreshold Model and Reverse Current. ....	30

## INTRODUCTION

Since 2004, when graphene was successfully exfoliated from graphite, numerous studies related to graphene, including one, two, and multiple layers, have been conducted. Following these advancements, several investigations have achieved the creation of metal-semiconductor junctions using the electrostatic gating method in single-layer graphene (SLG). An example of this is the fabrication of graphene-silicon Schottky diodes by depositing exfoliated graphene onto silicon substrates [1].

Among the key advantages of graphene, it stands out as an excellent candidate for next-generation FET transistors due to its high electron mobility and substantial capacity for electrical current transport [1]. Additionally, compared to other emerging structures such as nanotubes, graphene is more scalable and exhibits lower contact resistance.

Furthermore, graphene possesses high optical transparency, excellent surface conductivity, and outstanding mechanical and physical/chemical stability. These qualities make it a promising candidate for energy-related applications, including solar cells, lithium batteries, and supercapacitors. In [2], [3], and [4], these characteristics are leveraged to manufacture high-performance lithium batteries using silicon anodes in graphene. Similarly, in [5], Graphene Quantum Dots (GQDs) are used to form a heterojunction with crystalline silicon, leading to the development of highly efficient solar cells.

However, despite various applications of the graphene-silicon interface, a comprehensive understanding of the physics involved in the Schottky barrier between these two materials is yet to be achieved; therefore, it is essential to prioritize the physical study of the graphene-Si interface. The main objective of this work is to simulate the graphene-Si interface through quantum-mechanical and electrodynamic analyses to obtain a subthreshold model characterized by the current-voltage (IV) curve, enabling the comprehension of current

transport mechanisms at the junction through simulation results. Additionally, a crystallographic system containing the graphene-Si interface is constructed to obtain basic physical parameters.

This document is organized as follows: The first section consists of a brief introduction to the importance and applications of the graphene-Si interface, the second section introduces the state of the art through a literature review of [6] and the physics of devices background that was required for the development of this project, the third section presents the methodology employed, the fourth section shows the simulation results for the subthreshold model and IV curves, and the fifth section compiles the primary observations and findings of this study, and also proposes potential subjects for future research.

## STATE OF THE ART

### **Literature review: Vertically illuminated, resonant cavity enhanced, Graphene–Silicon Schottky photodetectors**

In the research paper by [6], photodetector sensors (PDs) were manufactured using graphene-Si Schottky diodes that operate with vertical illumination and exhibit enhanced resonant cavity, achieving efficient performance at 1550 nm. Through CMOS electronics, a promising approach to this application is feasible by enabling sub-bandgap photodetection in silicon and leveraging the internal photoemission process in a graphene-Si Schottky junction. The significance of these sensors lies in the importance of near-infrared (NIR) photodetection at 1550 nm for various fields and applications, ranging from optical communications to remote sensing.

The PDs were fabricated on a silicon substrate with a width of  $200\mu\text{m}$ , p-type, doped with a low boron concentration ( $N_A \sim 10^{15} \text{ cm}^{-3}$ ). These devices exhibit a rectifying I-V behavior that aligns with the Schottky diode equation. Subsection \ref{submodel} provides a

detailed comparison of the experimental curve described in [6] with the simulations obtained in this work. This comparison aims to validate the model obtained from the literature and to extend the understanding of the physical and electrodynamic behavior of the interface.

## Physics of Devices Background

### Effective Mass

The solution to the three-dimensional Schrödinger wave equation is the electron wave function [7].

$$-\frac{\hbar^2}{2m_0}\nabla^2\psi + V(\mathbf{r})\psi = E\psi \quad (1)$$

From (1), the electron's acceleration and its effective mass are described in (2) and (3):

$$\text{Acceleration} = -\frac{q\mathcal{E}}{\hbar^2} \frac{d^2E}{dk^2} \quad (2)$$

$$\text{Effective Mass} \equiv \frac{\hbar^2}{d^2E/dk^2} \quad (3)$$

When applying an electric field  $\mathcal{E}$ , an electron or a hole will be accelerated due to the laws of motion [7]:

$$\text{Acceleration} = -\frac{q\mathcal{E}}{m_*} \quad (4)$$

Where  $m_*$  can refer to the effective mass of electrons  $m_n$  or effective mass of holes  $m_p$ .

### Fermi Level

The Fermi level  $E_F$  is a measure of the maximum energy that can be occupied by electrons in a physical system. It is defined by the Fermi-Dirac distribution, which describes the probability of a quantum state being occupied by an electron at a given temperature [8].

$$f_F \approx \exp\left[-\frac{E - E_F}{kT}\right] \quad (5)$$

The Fermi level can also be expressed through the concentrations of electrons  $n$  and holes  $p$  [7], as seen in (6) and (7):

$$E_C - E_F = kT \cdot \ln\left(\frac{N_C}{n}\right) \quad (6)$$

$$E_F - E_V = kT \cdot \ln\left(\frac{N_V}{p}\right) \quad (7)$$

where  $N_C = 2 \left[\frac{2\pi m_n kT}{h^2}\right]^{3/2}$  and  $N_V = 2 \left[\frac{2\pi m_p kT}{h^2}\right]^{3/2}$  are the effective density of states of the conduction and valence bands, respectively.

### Band Structure

It represents the energy levels of solids and is used to determine whether a material is a conductor, semiconductor, or insulator. It is also used to establish whether the material presents direct or indirect band gaps, and to analyze the valence and conduction bands [9]. In this work, Density Functional Theory (DFT) simulations are performed to calculate the band structure of the graphene-Si crystalline structure conducted in Quantum ATK.

### Schottky Band Diagram

In a metal-semiconductor junction, the most important parameter is the Schottky barrier  $\Phi_B$ . Fig. 1 shows the band diagram of the Schottky junction. It is possible to identify the barrier  $\Phi_B$  between the metal and the semiconductor. There are two potential barriers:  $\Phi_{B_n}$  which prevents electron flow between metal and n-type semiconductor, and  $\Phi_{B_p}$ , which prevents hole flow between metal and p-type semiconductor [7]. In addition, it is possible to identify the depletion zone next to the interface, where the Fermi level is away conduction band  $n \approx 0$  and valence band  $p \approx 0$ .

Moreover, the parameter  $\Phi_B$  varies depending on the metal, as it is associated with

$$\Phi_{B_n} = \Psi_M - \chi_{Si} \quad (8)$$

where  $\Psi_M$  is the work function of the metal, and  $\chi_{Si}$  is the electron affinity of silicon [7].

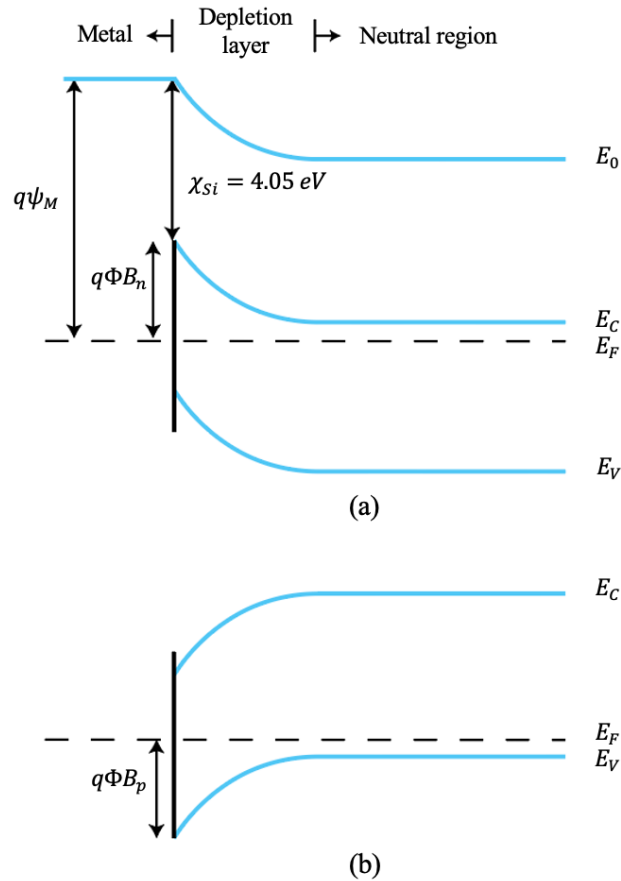


Figure 1. Band diagram of a metal-semiconductor junction. (a) n-type semiconductor. (b) p-type semiconductor. [7]

### Current Transport Mechanisms

At the metal-semiconductor junction, current transport primarily occurs through majority carriers, involving five basic processes [9]:

- (i) Thermionic emission of electrons from the semiconductor over the Schottky barrier  $\Phi_{B_n}$  to the metal.
- (ii) Quantum tunneling effect of electrons through the barrier.
- (iii) Recombination of electrons in the depletion region.

- (iv) Diffusion of electrons in the depletion region.
- (v) Holes injected from the metal into the semiconductor (equivalent to recombination in the neutral region).

In this work, the main focus is on transport mechanisms (i), (ii) and (iv).

### Thermionic Emission

Refers to the transport of electrons from the semiconductor to the metal, crossing over the Schottky barrier  $\Phi_{Bn}$  at an average velocity  $v_{thx}$ .

Equation [9] for current density describes this movement:

$$J_{S \rightarrow M} = \frac{1}{2} q n v_{thx} = A^* T^2 \exp \left[ -\frac{q\Phi_B}{kT} \right] \exp \left[ \frac{qV}{kT} \right] \quad (9)$$

where  $n = \frac{2\pi q m_n kT}{h^2} \exp \left[ \frac{-q(\Phi_B - V)}{kT} \right]$ , is the electron concentration,  $v_{thx} = \sqrt{2kT/\pi m_n}$ ,

and  $A^* = \frac{4\pi q m_n k^2}{h^3}$  is the effective Richardson constant. The term  $(\Phi_B - V)$  determines the amount of energy that electrons must have to overcome the barrier  $\Phi_B$  [7].

For the transport of electrons in the opposite direction, (10) is used [10], where the negative sign at the beginning indicates the direction:

$$J_{M \rightarrow S} = -A^* T^2 \exp \left[ -\frac{q\Phi_B}{kT} \right] \exp \left[ \frac{qV}{kT} \right] \quad (10)$$

Combining (9) and (10), the total current density is obtained:

$$J_n = J_{TE} \left[ \exp \left[ \frac{qV}{kT} \right] - 1 \right] \quad (11)$$

where  $J_{TE} = -A^* T^2 \exp \left[ -\frac{q\Phi_B}{kT} \right]$ .

### Diffusion

Refers to the transport of electrons from the semiconductor to the metal by diffusion in the depletion region. For this mechanism, in [10], the following conditions are assumed:

- (i) The height of the barrier  $\Phi_{B_n} \gg kT$ .
- (ii) The effect of electron collisions in the depletion region is included.
- (iii) The current flow does not affect carrier concentrations at  $x = 0$  and  $x = W$ .

From (12), which describes the dependence on the concentration gradient:

$$J_n = qD_n \left( \frac{n}{kT} \frac{dE_c}{dx} + \frac{dn}{dx} \right) \quad (12)$$

The term  $\exp\left[\frac{E_c(x)}{kT}\right]$  can be used as an integrating factor, and considering the boundary condition  $E_{F_m}$ , expression (13) is obtained:

$$J_n = \frac{qN_c D_n \left[ \exp\left[\frac{qV}{kT}\right] - 1 \right]}{\int_0^{W_D} \exp\left[\frac{E_c(x)}{kT}\right] dx} \quad (13)$$

Finally, considering (12) and (13) along with  $E_c(x) = q\Phi_{B_n} - \frac{q^2 N_D}{\epsilon_s} \left( W_D x - \frac{x^2}{2} \right)$ , the result is:

$$J_n = q\mu_n N_c \mathcal{E}_m \exp\left[-\frac{q\Phi_B}{kT}\right] \left[ \exp\left[\frac{qV}{kT}\right] - 1 \right] \quad (14)$$

$$J_n = J_D \left[ \exp\left[\frac{qV}{kT}\right] - 1 \right] \quad (15)$$

where (15) is very similar to (11); however, the saturation current density for diffusion  $J_D$  is bias-dependent and less sensitive to temperature [10].

### Thermionic-Emission-Diffusion

This is a synthesis of thermionic emission and diffusion proposed by Crowell and Sze.

This theory is derived from the thermionic recombination velocity boundary condition  $v_R$  near the metal-semiconductor interface [10]. From the above condition, we have

$$J = q(n_m - n_0)v_R \quad (16)$$

where  $n_m = N_c \exp\left[\frac{E_{F_n}(x_m) - q\Phi_{B_n}}{kT}\right]$  is the concentration of electrons at  $x_m$  when there is current.



On the other hand, another boundary condition considering  $E_{F_m} = 0$  is

$$E_{F_n}(W_D) = qV \quad (17)$$

Upon integrating the expression for  $E_{F_n}$  between  $x_m$  (maximum potential energy) and  $W_D$  (edge of the depletion region) [10], and considering (16) and (17),  $E_{F_n}(x_m)$  can be solved as follows

$$\exp\left[\frac{E_{F_n}(x_m)}{kT}\right] = \frac{v_D \exp\left[\frac{qV}{kT}\right] + v_R}{v_D + v_R} \quad (18)$$

where  $v_D$  is the effective velocity of electron diffusion from  $W_D$  to  $x_m$ .

Finally, by substituting (18) into (16), the result of the thermionic-emission-diffusion theory is obtained:

$$J_{TED} = \frac{qN_C v_R}{1 + \frac{v_R}{v_D}} \exp\left[-\frac{q\Phi_{Bn}}{kT}\right] \left[\exp\left[\frac{qV}{kT}\right] - 1\right] \quad (19)$$

where  $v_D \approx \mu n \mathcal{E}_m$  and  $v_R = \frac{A^* T^2}{qN_C}$ .

The complete expression for the  $J - V$  characteristics is thus:

$$J = A^{**} T^2 \exp\left[-\frac{q\Phi_{Bn}}{kT}\right] \left(\exp\left[\frac{qV}{kT}\right] - 1\right) \quad (20)$$

where  $A^{**}$  is the reduced Richardson constant.

### Tunnel Effect

Refers to the transport of electrons from the semiconductor to the metal through quantum tunneling across the Schottky barrier  $\Phi_B$ . The current density in (21) describes this process:

$$J_{S \rightarrow M} = \frac{A^{**} T^2}{kT} \int_{E_{F_m}}^{q\Phi_{Bn}} F_S T(E) (1 - F_M) dE \quad (21)$$

where  $T(E)$  is the tunneling probability, and  $F_S$  and  $F_M$  correspond to Fermi-Dirac distribution functions, indicating the occupation probability in the semiconductor and the unoccupied probability in the metal [10].

For the transport of electrons in the opposite direction, a similar expression to (21) is used, but with the factors  $F_S$  and  $F_M$  exchanged.

Additionally, Fig. 2 shows the three components of the tunneling current which, according to [10], are:

- (i) Thermionic Emission (TE)
- (ii) Field Emission near the Fermi level (FE) - Pure tunneling process
- (iii) Thermionic-Field Emission (TFE) between TE and FE - Tunneling of thermally excited carriers, where the  $\Phi_B$  barrier is thinner than for FE.

Finally, the overall current density can be calculated by taking into account (11) and (21) as shown below:

$$J = J_0 \left[ \exp \left[ \frac{qV}{\eta kT} \right] - 1 \right] \quad (22)$$

where  $J_0$  refers to the saturation current density and  $\eta$  represents the ideality factor associated to the slope.

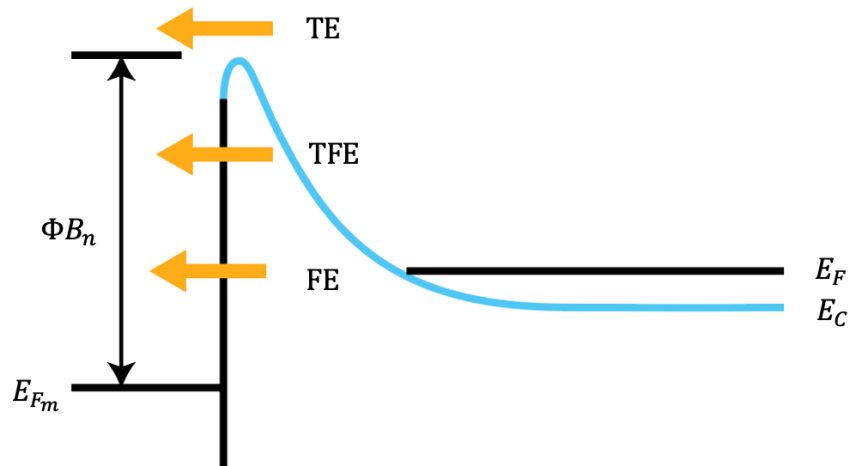


Figure 2. Tunneling current components. [10]

## METHODOLOGY

The methodology employed for this work is divided into two levels:

The first level involves the quantum-mechanical analysis of the graphene-Si interface. To carry out this analysis, the High-Performance Computing (HPC) server and Quantum ATK software from Synopsis are utilized to approximate Schrodinger's equation using the Density Functional Theory (DFT).

DFT is a quantum-mechanical simulation method used in solid-state physics to calculate the properties of an atomic system: molecules, crystals, and surfaces [11]. In DFT, the Born-Oppenheimer equation is used to approximate Schrodinger's equation by analyzing electronic and nuclear movements separately.

The second level comprises the electronic analysis of the graphene-Si interface. To conduct this electrodynamic analysis, the results obtained from the quantum-mechanical analysis are used, and a device that meets the specified characteristics is replicated in the Synopsis Sentaurus software. At this level, a mesh of various points is generated in the device, where Poisson's equation, coupled to the drift-diffusion model, is solved to obtain the IV curves that characterize the junction.

Poisson's equation describes the distribution of electric potential in an electric field, using the formula:

$$\nabla^2\phi = -\frac{\rho}{\epsilon} \quad (23)$$

where  $\phi$  is the electric potential,  $\rho$  is the electric charge density, and  $\epsilon$  is the electric permittivity of the material [12]. The solution to this equation is of great relevance for the modeling and analysis of electronic devices and semiconductors.

## RESULTS

### Formation of the crystal supercell – QuantumATK

The crystal supercell is formed from the primitive cells of silicon and graphene. Fig. 3 shows the base vectors  $\mathbf{a1}$  and  $\mathbf{a2}$ , which define the area of one side of the primitive cells. To build the structure, it is necessary to couple both areas using the scalar factors  $M$  and  $M''$ , ensuring that both the areas of silicon and graphene are mutually contained and/or have similar values. The values  $\mathbf{a1}''$  (A) and  $\mathbf{a2}''$  (B) resulting from the multiplication of the silicon base vectors by  $M$  and the graphene base vectors by  $M''$  are used to construct the 2D space of the crystal supercell. A fitting parameter,  $C$ , is then introduced for the third dimension, which must provide at least 15 Å of vacuum. This process ensures a coherent and efficient integration of silicon and graphene in the final crystal supercell.

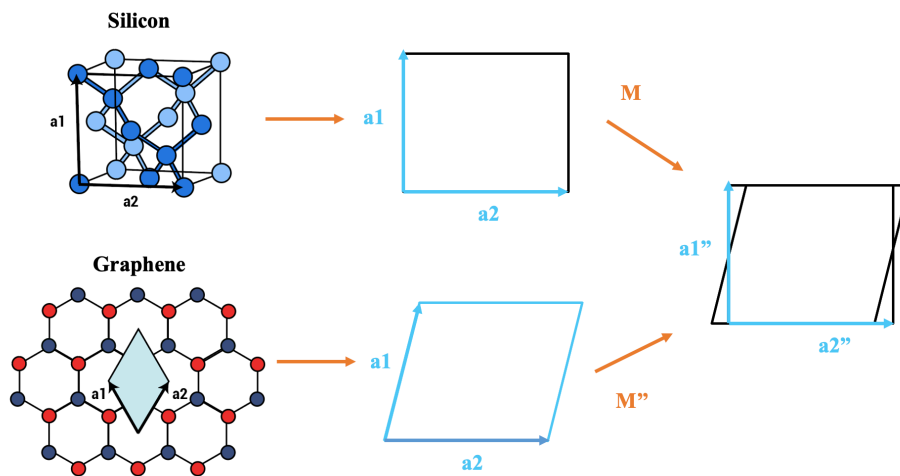


Figure 3. Formation of the graphene-Si crystal supercell.

Finally, the three parameters  $A$ ,  $B$ , and  $C$  are adjusted until convergence is reached in the VASP software, ensuring the correct configuration and stability of the obtained crystal structure. Fig. 4 depicts the crystal supercell in QuantumATK while Table 1 shows the final values of  $A$ ,  $B$ , and  $C$  and the scalar factors  $M$  and  $M''$ , together with the areas of the silicon and graphene cells, and the structure.

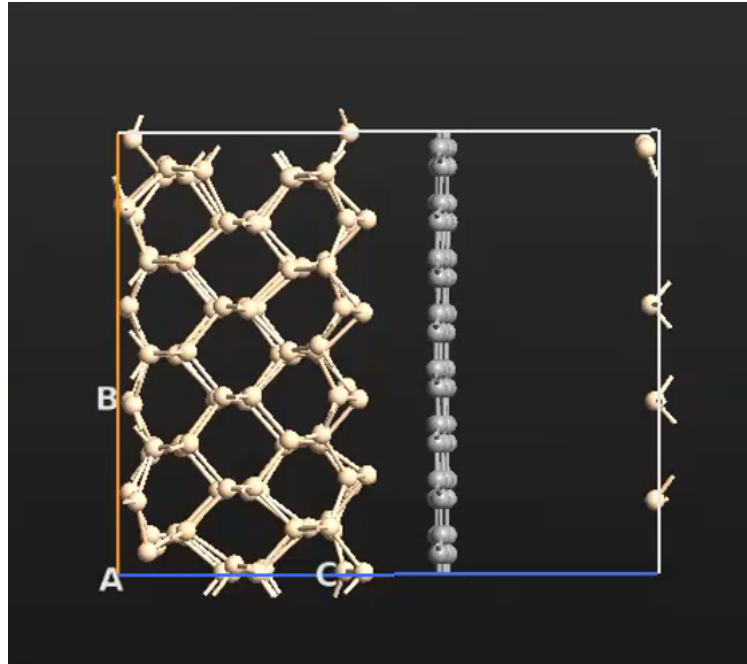


Figure 4. Graphene-Si crystal supercell - Optimized configuration.

Parameters	Silicio $\times$ M	Grafeno $\times$ M''
A = 12.075 Å	3.83 $\times$ 3	3.83 $\times$ 5
B = 17.802 Å	2.474 $\times$ 5	1.428 $\times$ 13
C = 21.365 Å	15 Å of empty space	
Area = A $\times$ B 214.96 Å <sup>2</sup>	<b>220.03 Å<sup>2</sup></b>	<b>229.63 Å<sup>2</sup></b>

Table 1. Parameters of the crystal supercell.

### Parameter Extraction of the Graphene-Si Interface - QuantumATK

First, a quantum mechanical study was conducted to determine the impact of a graphene sheet on the electronic structure of a silicon crystal. The study identifies the characteristics of the optimized configuration of the crystal and analyzes the changes caused by the displacement of the graphene layer. By employing the DFT in plane wave simulations, the band structure, effective mass, and Fermi level are calculated in every simulation for a quantitative and qualitative comparison.

For the optimized configuration, exhibited in Fig. 4, the graphene sheet was placed 1.45 Å away from the Si crystal. The band structure obtained for this configuration is displayed in

Fig. 5(a). It is evident that the conduction and valence bands are closely located, resulting in the absence of a band gap. As a result, it is confirmed that the graphene sheet acts as a metal since electrons can move freely from the valence to the conduction band.

Next, the graphene layer was displaced by  $-1 \text{ \AA}$ , positioning it at a distance of  $0.45 \text{ \AA}$  from the Si crystal. The band structure portrayed in Fig. 5(b) suggests that for this configuration the metal properties of graphene have been intensified since the conduction and valence bands are closer together and more flattened, resulting in electrons moving even more freely between bands, and thus, more direct conduction.

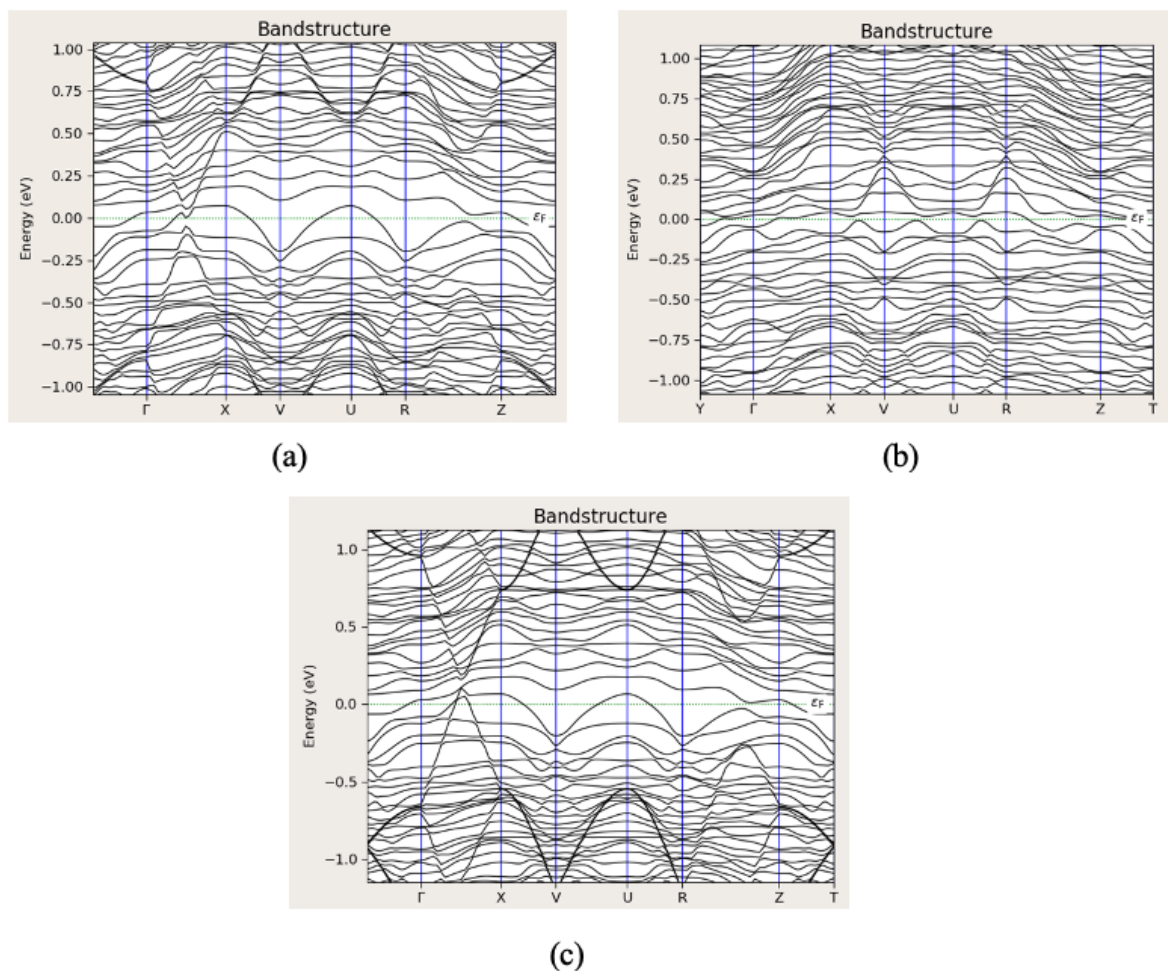


Figure 5. Band Structure of the graphene layer. (a) Optimized configuration. (b)  $-1 \text{ \AA}$  displacement. (c)  $+2.5 \text{ \AA}$  displacement.

Subsequently, the graphene sheet was displaced  $+2.5 \text{ \AA}$  from the optimized configuration, placing it at  $3.95 \text{ \AA}$  away from the Si crystal. In this case, the band structure from Fig. 5(c) shows a change in the properties of the graphene layer. Since now there is a clear distance between the conduction and valence bands, with band gaps of approximately  $110 \text{ meV}$ , it can be established the graphene sheet exhibits less metal properties. Consequently, electrons cannot move as freely between bands.

Finally, the effects of displacing the graphene sheet can also be observed in the Fermi level and effective mass. When the graphene sheet is closer to the Si crystal, the Fermi level, work function, and effective mass decrease, whereas when the graphene sheet is further from the Si crystal, these values increase. A summary of the results is presented in Table 2.

Configuration	Fermi level / Work Function (eV)	Effective mass $m_*(m_e)$
Optimized	4.781765	0.859
-1 $\text{\AA}$	4.615097	0.187
+2.5 $\text{\AA}$	4.815251	0.882

Table 2. Physical Parameters of the Graphene Layer

### Device Construction: Mesh and Doping – Sentaurus

In the second step, the graphene-Si Schottky device was constructed using Sentaurus software. The metal-semiconductor diode consisted of a graphene layer with varying widths (5nm, 10nm, 100nm, and 500nm), and a p-type, low-doped,  $1 \mu\text{m}$  thick Si substrate. The doping concentration was set to  $N_A = 10^{15}$ , Boron, as per the outlined device description in [6].

Fig. 6 shows an example of the Schottky diode, with a graphene width of 5nm, and its respective mesh. It is important to mention that the mesh was proportionately constructed to the diodes' different sizes with special emphasis on the interface, where the great majority of points need to be concentrated.

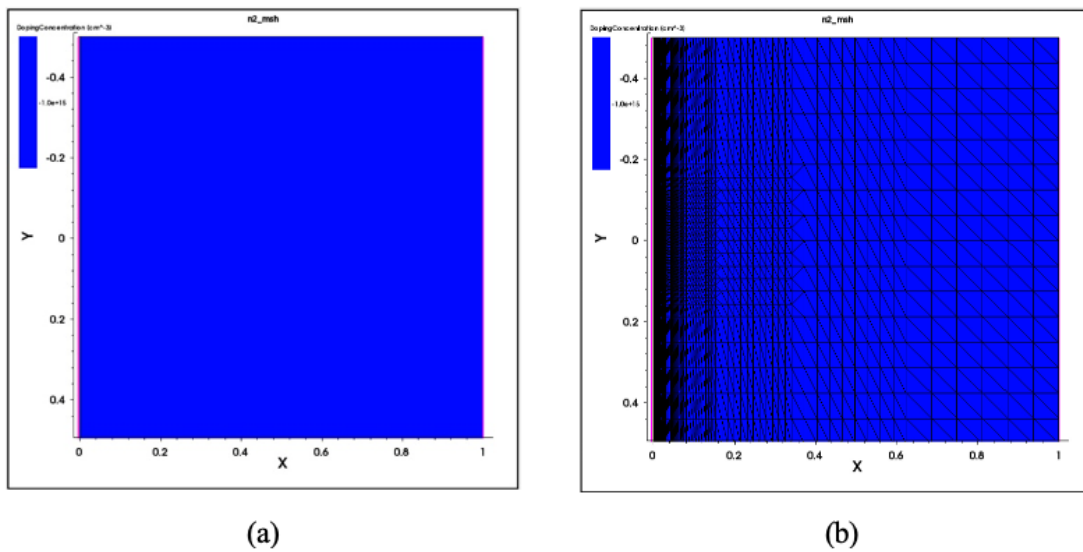


Figure 6. Graphene-Si Schottky Diode in Sentaurus, Graphene = 5nm (wide), Si = 1  $\mu$ m (wide).

### Creation of the Graphene Material – Sentaurus

Since it was determined in Fig. 5(a) that the graphene layer in the crystallographic system behaves like a metal, the parameter file for graphene in the present TCAD model was created based on the default parameter file for metals available in Sentaurus.

In said file, the parameters included were collected from Quantum-ATK (DFT) and the literature, as listed below:

- Monolayer Graphene's lumped electron-hole-lattice heat capacity at 300K corresponds to  $C_V = 6.58 (J/K \cdot cm^3)$  [13].
- Graphene's lattice thermal conductivity has a value of  $\kappa = 29 (W/K \cdot cm)$  [14].
- The effective mass of graphene obtained from Quantum-ATK simulations is  $m_* = 0.859m_e$ , as mentioned in Table 2.
- The work function ( $\Psi_M$ ) and Fermi energy were also obtained from Quantum-ATK simulations. Since in metals both these parameters have the same value,  $\Psi_M = \text{Fermi level} = 4.781765 (eV)$ , as displayed in Table 2; which is similar to the value found in literature [15].



- The resistivity of graphene is  $\rho = 0.2 \times 10^{-3} (\Omega \cdot cm)$  [16].
- The temperature coefficient of graphene is  $\alpha = 2.07 \times 10^{-3} (1/K)$  [17].

#### IV Curves due to Thermionic Emission

The initial simulations were performed for an applied voltage  $V_a$  ranging from -0.5 V to 0.5 V, and for different values of recombination velocity of holes:  $v_{rh} = 1 \times 10^2 (cm/s)$  and  $1 \times 10^3 (cm/s)$ .

Fig. 7 displays the results on a semi-logarithmic scale. The calculated subthreshold slope for both curves is  $SS = 60 (mV/decade)$ , which can be explained through (11) (Thermionic Emission Theory). In both cases, the overall current in  $\backslash\text{eqref}\{\text{allcurrent}\}$  has an ideality factor of  $\eta = 1$  since the  $SS$  value does not deviate from the standard. Additionally, it is evident that an increase in recombination velocity leads to a higher saturation current.

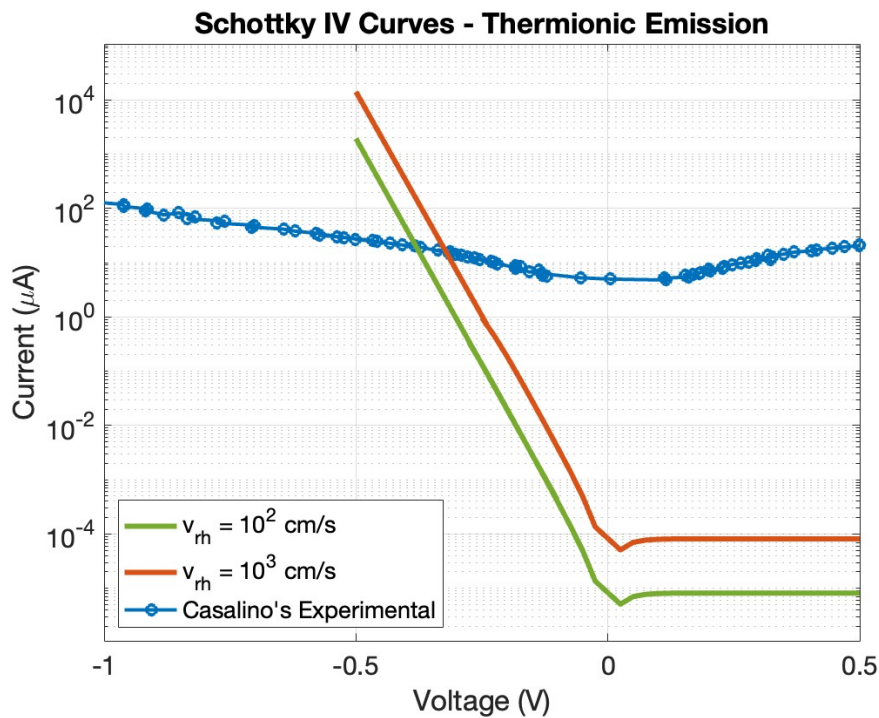


Figure 7. IV Curves due to Thermionic Emission - Semilog scale.

These findings were consistent across all the variously sized TCAD models explained in Subsection *Device Construction* since the primary occurrences take place at the graphene-Si interface. Henceforth, the Schottky diode with a graphene width of 5nm is regarded as the primary device for analysis.

When compared to Casalino's IV fitting in [6], it was determined that the simulation did not fit the experimental curve. Thus, it is necessary to adjust the parameters  $v_{rh}$  and tunneling current to increase the  $SS$  and thereby,  $\eta$ .

#### IV Curves due to Diffusion and Tunneling

The next set of simulations was also performed for a  $V_a$  ranging from -0.5 V to 0.5 V, and for increased values of recombination velocity of holes:  $v_{rh} = 2 \times 10^6$  (cm/s) and  $2.2 \times 10^7$  (saturation). The new values for  $v_{rh}$  were selected according to the theory explained in [7] and [10], and considering (16) and (19).

Fig. 8 exhibits the results on a semi-logarithmic scale. In both cases,  $SS$  and  $\eta$  have notably increased for both curves, yellow and violet, to  $SS = 572$  (mV/decade),  $\eta \approx 10$ , and  $SS = 585$  (mV/decade),  $\eta \approx 10$ , respectively, which can be sustained by (19) (Thermionic-Emission-Diffusion Theory). For this scenario, since  $v_{rh} = v_R$  is considerably high and in saturation, it is possible to assert that  $v_R \gg v_D$ ; therefore, as stated in [10], the pre-exponential factor in (19) is dominated by  $v_D$ , which implies the limiting factor is  $J_{TED} = J_D$  (Diffusion).

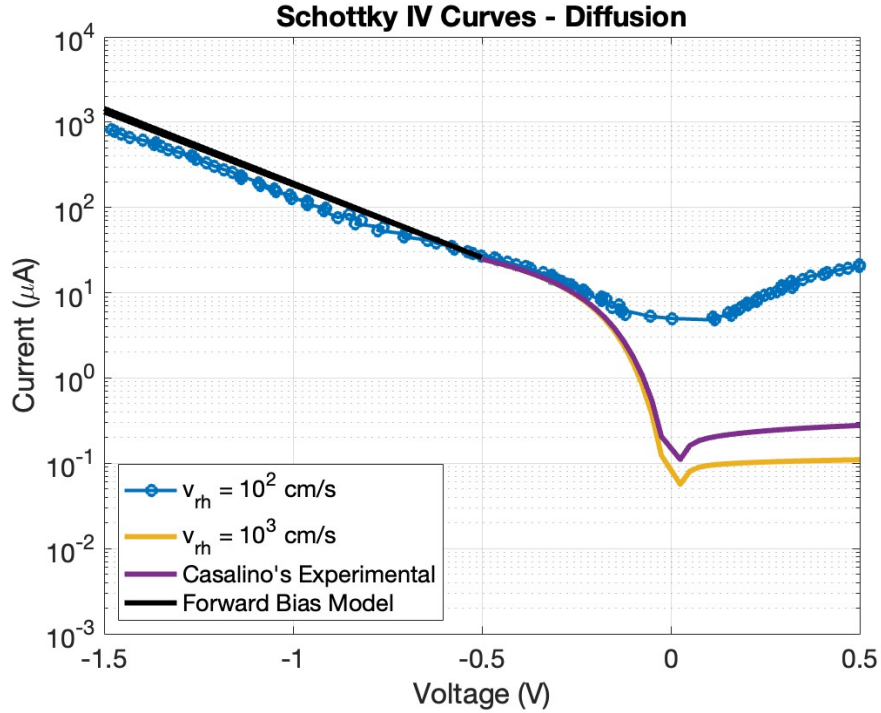


Figure 8. IV Curves due to Diffusion - Semilog scale.

Moreover, Fig. 9 shows the effect of the width of the tunnel in the current for  $W_T = 1\text{ nm}$ ,  $10\text{ nm}$ ,  $100\text{ nm}$ , and  $1\mu\text{ m}$ . As demonstrated in (21), an increase in the tunneling probability  $T(E)$  results in a greater contribution to the current generated by the tunnel effect. The value of  $T(E)$  is directly influenced by  $W_T$ ; therefore, it can be observed that Schottky models exhibiting higher  $W_T$  values yield higher values of  $T(E)$ , which in turn increases  $SS$  and  $\eta$ .

The result that best fits the experimental curve in [6] is the curve corresponding to  $W_T = 1\mu\text{ m}$  since  $W_T$  covers the entire width of the semiconductor in the Schottky diode. The defining parameters of this curve are  $SS = 666$  (mV/decade) and  $\eta \approx 11$ .

In both Fig. 8 and Fig. 9, the Forward Bias Model is also added through extrapolation for a  $V_a$  range of  $-1.5\text{ V}$  to  $-0.5\text{ V}$ . The results reveal that as the value of  $\eta$  approaches 11, the extrapolation aligns more closely with Casalino's Forward Bias fitting, as detailed in [6].

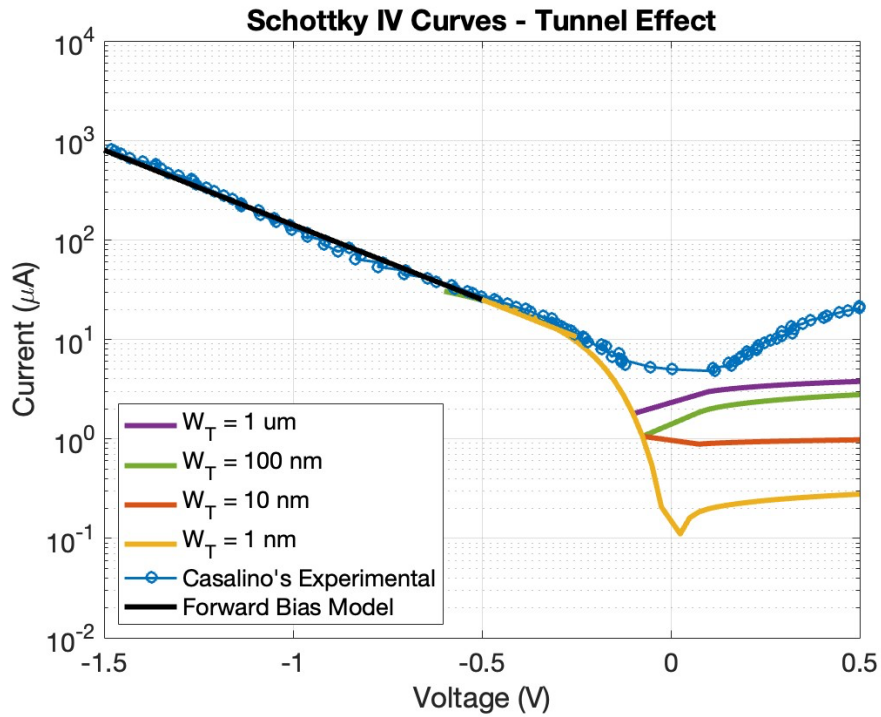


Figure 9. IV Curves due to Tunneling - Semilog scale.

Furthermore, Fig. 10 depicts the primary tunneling current, which occurs due to the concentration of electron tunneling at the graphene-Si interface.

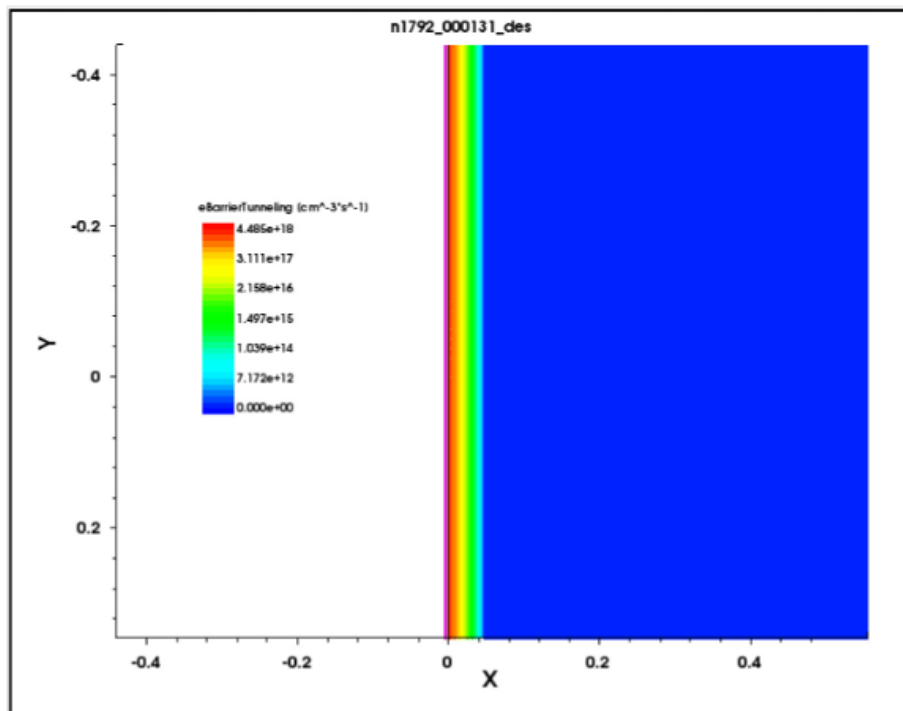


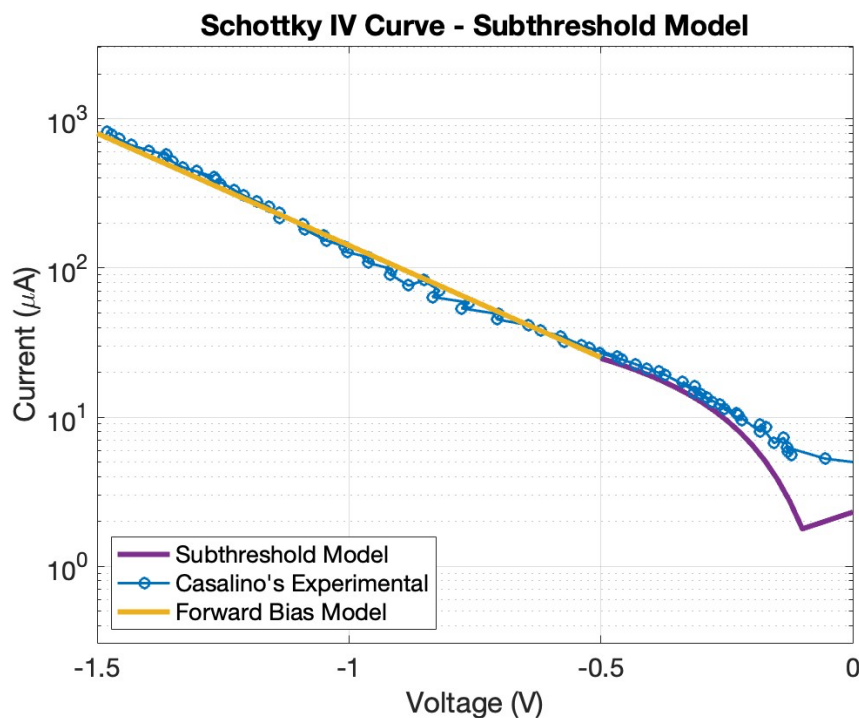
Figure 10. Tunnel Effect in the Schottky diode.

### Subthreshold Model

A subthreshold model can be formulated based on the defining parameters acquired in Subsection *IV Curves due to Diffusion and Tunneling*.

Fig. 11(a) depicts the subthreshold model along with the extrapolation for the forward bias model, while Fig. 11(b) illustrates the subthreshold model with the reverse current. Through Fig. 11(a), the contribution of the different transport mechanisms to the subthreshold current in the Schottky diode was established as: 80.42% to Thermionic-Emission-Diffusion Theory (dominated by diffusion) and 19.58% to Tunneling.

For the overall current, however, both Fig. 11(a) and Fig. 11(b) show that the contributions of the different transport mechanisms can be divided as: 62.38% to Thermionic-Emission-Diffusion Theory (80.16% in Forward Bias and 19.84% in Subthreshold), and 37.62% to Tunneling (33.55% in Subthreshold and 66.45% in Reverse Bias).



(a)

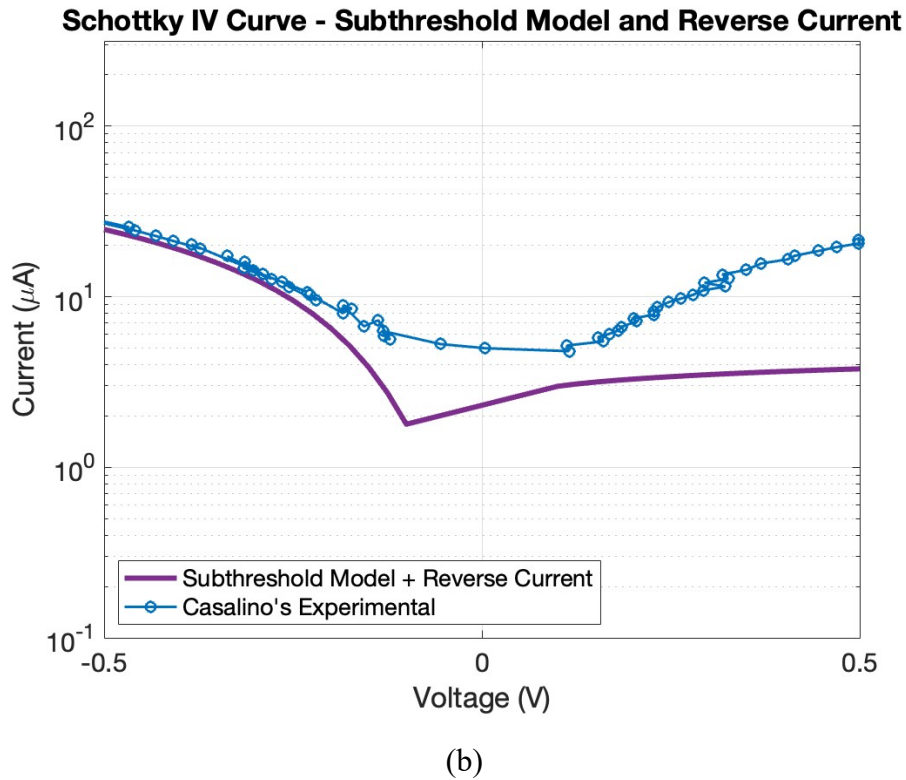


Figure 11. Schottky IV Curve. (a) Subthreshold Model. (b) Subthreshold Model and Reverse Current.

When comparing this final curve to Casalino's fitting in [6], the Forward Bias Model curve is nearly identical to the experimental curve in the range from -1.5 V to -0.5 V, with a percent error of 1.11%, the Subthreshold Model curve in the range from -0.5 V to 0 V has a percent error of 4.74%, and the reverse current curve in the range from 0 V to 0.5 V has a percent error of 9.35%.

Additionally, Fig. 12(a) shows the band diagram for the Schottky diode when  $V_a = 0$ . The calculated Schottky barrier corresponds to  $|\Phi_{B_0}| = 0.46$  V. Likewise, Fig. 12(b) shows the band diagram when  $V_a = -0.5$  V. In this case,  $\Phi_{B_0}$  decreases, allowing the hole current to flow through the device.

Finally, Table 3 summarizes the parameters of the obtained subthreshold model and compares them with those specified in Casalino's experimental curve. Notably, the key parameters of

the subthreshold model, which impact the diode current:  $SS$ ,  $\eta$ , and  $\Phi_B$ , closely match those found in [6].

Parameter	Subthreshold Model [This work]	Experimental Curve Casalino [6]
$v_{rh}$	$2.2 \times 10^7$ (cm/s)	$3.83 \times 5$
$W_T$	1 $\mu\text{m}$	$1.428 \times 13$
$SS$	666 (mV/decade)	685 (mV/decade)
$\eta$	0.41 eV	0.46 eV
Area	1.005 $\mu\text{m}^2$	$\pi \times 10^{-4}$ $\text{cm}^2$

Table 3: Comparison of Subthreshold Model parameters with Casalino's experimental curve.

## CONCLUSIONS AND FUTURE WORK

The significance of a T-CAD model for a Schottky diode with a Graphene/Silicon interface lies in its applicability to a wide range of integrated and embedded circuit designs. This model allows for the simulation of various circuits, and its electronic behavior closely aligns with experimental observations.

Another crucial aspect is the insights gained into the physics of the device. The T-CAD model provides a deeper understanding of the device's behavior, aiding in the optimization of parameters like the IV curve, subthreshold slope, Schottky barrier, and more, for enhanced electronic performance.

The final results obtained for the subthreshold model with the p-type, boron-doped Schottky are comparable to those exhibited by Casalino in \cite{Casalino2017}. The values obtained can be summarized in a subthreshold slope  $SS$  of 666 mV/decade ( $\eta = 11$ ), with an 80.42% contribution of Thermionic-Emission-Diffusion Theory (dominated by diffusion) and a 19.58% contribution of Tunneling.

The percent errors obtained between the simulated curve and Casalino's experimental curve were 1.11% in Forward Bias, 4.74% in Subthreshold, and 9.35% in Reverse Bias.

The Subthreshold Model, when combined with the Forward Bias Model, accurately represents the forward current, which is the region of interest since it is the main region of application for Schottky diodes, including rectifiers and photodetectors.

For future work, the simulation's range could be expanded to include the Forward Bias and/or Reverse Bias regions, in order to gain a more thorough understanding of the physics and electrostatics that govern the graphene-Si interface. Moreover, an interface comprising graphene-intrinsic silicon and/or graphene-amorphous silicon could also be developed for study, simulation, and characterization.



## REFERENCES

- [1] C.-C. Chen, M. Aykol, C.-C. Chang, A. F. J. Levi, and S. B. Cronin, “Graphene-Silicon Schottky Diodes,” *Nano Letters*, vol. 11, no. 5, pp. 1863–1867, May 2011, doi: 10.1021/nl104364c.
- [2] Z. Ma *et al.*, “Crucial contact interface of Si@graphene anodes for high-performance Li-ion batteries,” *Applied Surface Science*, vol. 603, p. 154383, Nov. 2022, doi: 10.1016/j.apsusc.2022.154383.
- [3] S. Basu *et al.*, “Utilizing van der Waals Slippery Interfaces to Enhance the Electrochemical Stability of Silicon Film Anodes in Lithium-Ion Batteries,” *ACS Applied Materials & Interfaces*, vol. 10, no. 16, pp. 13442–13451, Apr. 2018, doi: 10.1021/acsami.8b00258.
- [4] D. Lou *et al.*, “Scalable fabrication of Si-Graphene composite as anode for li-ion batteries,” *Applied Sciences*, vol. 12, no. 21, p. 10926, Oct. 2022, doi: 10.3390/app122110926.
- [5] P. Gao *et al.*, “Crystalline SI/Graphene quantum dots heterojunction solar cells,” *Journal of Physical Chemistry C*, vol. 118, no. 10, pp. 5164–5171, Mar. 2014, doi: 10.1021/jp412591k.
- [6] M. Casalino *et al.*, “Vertically illuminated, resonant cavity enhanced, Graphene–Silicon Schottky photodetectors,” *ACS Nano*, vol. 11, no. 11, pp. 10955–10963, Nov. 2017, doi: 10.1021/acsnano.7b04792.
- [7] C. Hu, *Modern semiconductor devices for integrated circuits*. Prentice Hall, 2010.
- [8] D. A. Neamen, *Semiconductor Physics and Devices*. McGraw-Hill Education, 2011.
- [9] W. Xia and L. A. R. Pestana, *Fundamentals of multiscale modeling of structural materials*. Elsevier, 2022.

- [10] S. M. Sze and K. K. Ng, *Physics of semiconductor Devices*. John Wiley & Sons, 2006.
- [11] Synopsis, “What is density functional Theory and how does it work?,” *Density Functional Theory*, 2021. <https://www.synopsys.com/glossary/what-is-density-functional-theory.html>
- [12] F. Ulaby and U. Ravaioli, *Fundamentals of Applied Electromagnetics*, 7th ed. Pearson Education, 2015.
- [13] V. Ryzhii, M. Ryzhii, T. Otsuji, V. Mitin, and M. S. Shur, “Heat capacity of nonequilibrium electron-hole plasma in graphene layers and graphene bilayers,” *Physical Review*, vol. 103, no. 24, Jun. 2021, doi: 10.1103/physrevb.103.245414.
- [14] L. F. C. Pereira, “Investigating mechanical properties and thermal conductivity of 2D carbon-based materials by computational experiments,” *Computational Materials Science*, vol. 196, p. 110493, Aug. 2021, doi: 10.1016/j.commatsci.2021.110493.
- [15] E. V. Rut’kov, E. Yu. Afanas’eva, and N. R. Gall, “Graphene and graphite work function depending on layer number on Re,” *Diamond and Related Materials*, vol. 101, p. 107576, Jan. 2020, doi: 10.1016/j.diamond.2019.107576.
- [16] H. Liu, A. S. Deshmukh, N. Salowitz, J. Zhao, and K. Sobolev, “Resistivity signature of Graphene-Based Fiber-Reinforced composite subjected to mechanical loading,” *Frontiers in Materials*, vol. 9, Jan. 2022, doi: 10.3389/fmats.2022.818176.
- [17] H. Liu, A. S. Deshmukh, N. Salowitz, J. Zhao, and K. Sobolev, “Resistivity signature of Graphene-Based Fiber-Reinforced composite subjected to mechanical loading,” *Frontiers in Materials*, vol. 9, Jan. 2022, doi: 10.3389/fmats.2022.818176.

## ANNEX A: CODE 1 - SDE\_DVS.CMD

```

; Reinitializing SDE
(sde:clear)
; set coordinate system up direction
(sde:set-process-up-direction "+z")

; Selecting default Boolean expression
(sdegeo:set-default-boolean "ABA")

; Creating rectangular regions
(sdegeo:create-rectangle
  (position 0 -0.50 0.0) (position 1.00 0.50 0.0) "Silicon" "R.Doping")
(sdegeo:create-rectangle
  (position -@Tint@ -0.50 0.0) (position 0.0 0.50 0.0) "Metal" "R.Metal")

.*****

; Creating single-lumped regions
(sde:assign-material-and-region-names "all")

.*****

; Defining contacts

(sdegeo:define-contact-set "top" 4 (color:rgb 1 0 0) "##")
(sdegeo:define-contact-set "bottom" 4 (color:rgb 0 1 0) "##")

(sdegeo:set-contact (find-edge-id (position -@Tint@ 0.0 0.0)) "top")
(sdegeo:set-contact (find-edge-id (position 1.00 0.0 0.0)) "bottom")

.*****

(sdedr:define-constant-profile "Const.P" "BoronActiveConcentration" 1e15)
(sdedr:define-constant-profile-region "PlaceCD.P" "Const.P" "R.Doping")

; Saving the model
(sde:save-model "n@node@")

.*****

;-----
;-- Specify mesh refinements -----
;-----

; Defining the global refinement window
(sdedr:define-refeval-window "RefWin.all" "Rectangle" (position -@Tint@ -0.50 0) (position 1 0.50 0))
(sdedr:define-refinement-size "RefDef.all" 0.25 0.10 0.25 0.20)
(sdedr:define-refinement-placement "PlaceRF.all" "RefDef.all" "RefWin.all")
(sdedr:define-refinement-function "RefDef.all" "MaxLenInt" "Metal" "Silicon" 0.001 1.1 "DoubleSide")

(sdedr:define-refeval-window "RefWin.interface" "Rectangle" (position (/ @Tint@ -50.00) (* -@Tint@ 20.00) 0.0) (position (/
@Tint@ 50.00) (* @Tint@ 20.00) 0.0))
(sdedr:define-refinement-size "RefDef.interface" (/ @Tint@ 5.00) (/ @Tint@ 15.00) (/ @Tint@ 25.00) (/ @Tint@ 100.00))
(sdedr:define-refinement-placement "PlaceRF.interface" "RefDef.interface" "RefWin.interface")

; Meshing the device structure
(sde:build-mesh "n@node@")

```

## ANNEX B: CODE 2 - METAL.PAR OR GRAPHENE MODEL

\* Copyright (c) 1994-2022 Synopsys, Inc.  
 \* This parameter file and the associated documentation are proprietary to Synopsys, Inc. This parameter file may  
 \* only be used in accordance with the terms and conditions of a written license agreement with Synopsys, Inc. All  
 \* other use, reproduction, or distribution of this parameter file is strictly prohibited.

```

Epsilon
{ * Ratio of the permittivities of material and vacuum
  * epsilon() = epsilon
    epsilon = 0.0000e+00 # [1]
}
Epsilon_Inf
{ * Ratio of the high frequency limit of permittivities of material and vacuum
  * epsilon_inf() = epsilon_inf
    epsilon_inf = 0.0000e+00 # [1]
}
Epsilon_aniso
{ * Ratio of the permittivities of material and vacuum
  * epsilon() = epsilon
    epsilon = 0.0000e+00 # [1]
}
Epsilon_Inf_aniso
{ * Ratio of the high frequency limit of permittivities of material and vacuum
  * epsilon_inf() = epsilon_inf
    epsilon_inf = 0.0000e+00 # [1]
}

RefractiveIndex
{ * Optical Refractive Index
  * refractiveindex() = refractiveindex * (1 + alpha * (T-Tpar))
    Tpar = 3.0000e+02 # [K]
    refractiveindex = 0.0000e+00 # [1]
    alpha = 2.0000e-04 # [1/K]
  * Gain dependence of refractive index in active region:
  * a) Linear model: delta n = a0 * ( (n+p)/(2 * N0) - 1 )
  * b) Logarithmic model: delta n = a0 * log ( (n+p)/(2 * N0) )
  * where n/p are the carrier densities in the active region.
    a0 = 0.0000e+00 # [1]
    N0 = 1.0000e+18 # [1/cm^3]
}

ComplexRefractiveIndex
{ * Complex refractive index model: n_complex = n + i*k (unitless)
  * with n = n_0 + delta_n_lambda + delta_n_T + delta_n_carr + delta_n_gain
  * k = k_0 + delta_k_lambda + delta_k_carr
  * Base refractive index and extinction coefficient:
  * n_0, k_0
  * Wavelength dependence (real and imag):
  * Formula 0: delta_n_lambda = Cn_lambda * lambda + Dn_lambda * lambda^2
  * delta_k_lambda = Ck_lambda * lambda + Dk_lambda * lambda^2
  * Formula 1: Read tabulated values
  * NumericalTable (...)
  * Formula 2: Read tabulated values from file
  * NumericalTable = <string>
  * Temperature dependence (real):
  * delta_n_T = n_0 * ( Cn_temp * (T-Tpar) )
  * Carrier dependence (real)
  * delta_n_carr = - Cn_carr * (const.) * (n/m_e + p/m_h)
  * Carrier dependence (imag)
  * delta_k_carr = 1 / (4*PI) * (wavelength^Gamma_k_carr_e * Ck_carr_e * n * wavelength
  * ^Gamma_k_carr_h * Ck_carr_h * p)
  * Gain dependence (real)
  * lin: delta_n_gain = Cn_gain * ( (n+p)/(2 * Npar) - 1 )
  * log: delta_n_gain = Cn_gain * log ( (n+p)/(2 * Npar) )
    n_0 = 1 # [1]
    k_0 = 0.0000e+00 # [1]
    Cn_lambda = 0.0000e+00 # [um^-1]
    Dn_lambda = 0.0000e+00 # [um^-2]
    Ck_lambda = 0.0000e+00 # [um^-1]
    Dk_lambda = 0.0000e+00 # [um^-2]
}

```

```

    Cn_temp = 2.0000e-04    # [K^-1]
    Cn_carr = 1            # [1]
    Ck_carr = 0.0000e+00,  0.0000e+00    # [cm^2]
    Gamma_k_carr = 1,      1            # [1]
    Cn_gain = 0.0000e+00  # [1]
    Npar = 1.0000e+18     # [cm^-3]
    Formula = 0
    Tpar = 3.0000e+02     # [K]
}

LatticeHeatCapacity
{ * lumped electron-hole-lattice heat capacity
  * cv() = cv + cv_b * T + cv_c * T^2 + cv_d * T^3
    cv = 6.58            # [J/(K cm^3)]
  * Heat capacity of nonequilibrium electron-hole plasma in graphene layers and graphene bilayers
    cv_b = 0.0000e+00    # [J/(K^2 cm^3)]
    cv_c = 0.0000e+00    # [J/(K^3 cm^3)]
    cv_d = 0.0000e+00    # [J/(K^4 cm^3)]
}

Kappa
{ * Lattice thermal conductivity
  * Formula = 0:
    * kappa() = 1 / ( 1/kappa + 1/kappa_b * T + 1/kappa_c * T^2 )
  * Formula = 1:
    * kappa() = kappa + kappa_b * T + kappa_c * T^2
  Formula = 1
    kappa = 29           # [W/(K cm)]
}
* Investigating mechanical properties and thermal conductivity of 2D carbon-based materials by computational experiments
    kappa_b = 0.0000e+00  # [W/(K^2 cm)]
    kappa_c = 0.0000e+00  # [W/(K^3 cm)]
}
* AllDependent Thermal Conductivity
    wL_n = 0.2            # [1]
    wL_p = 0.02          # [1]
    wT_n = 8              # [1]
    wT_p = 6              # [1]
    wTU_n = 9.0000e+05   # [1]
    wTU_p = 2.0000e+06   # [1]
    b = 1.8600e+02       # [1]
    M_n = 30.9            # [Da]
    M_p = 10.8            # [Da]
    R_n = 1.2300e-10     # [m]
    R_p = 1.1700e-10     # [m]
    r_del = 1            # [1]
    Ax = 0.0000e+00     # [s^3]
    eta = 1.5000e-10    # [m]
    Eu_n = 9              # [eV]
    Eu_p = 45             # [eV]
    ED_n = 1.33          # [eV]
    ED_p = 1.33          # [eV]
    dLy = 0.3            # [m]
    Lb = 7.1600e-03      # [m]
    Q_n = 4               # [1]
    Q_p = 15              # [1]
    Nomg = 3              # [1]
    order = 2             # [1]
    epsilon = 11.7        # [F/cm]
    m_c = 0.9             # [kg]
    m_v = 0.58            # [kg]
    rho = 2.3290e+03     # [kg/m^3]
    BL = 2.0000e-24      # [s/K^3]
    BT = 9.3000e-13      # [1/K^4]
    BTU = 5.5000e-18     # [s]
    omega1 = 2.3570e+13   # [1/s]
    omega2 = 2.7490e+13   # [1/s]
    omega3 = 7.4630e+13   # [1/s]
    omega4 = 4.5820e+13   # [1/s]
    M_h = 28              # [Da]
    R_h = 1.4600e-10     # [m]
    V_h = 1.2100e-05     # [m^3/mol]
    vL = 8.4800e+03      # [m/s]
    vLp = 4.2400e+03     # [m/s]
    vT = 5.8600e+03      # [m/s]
    vTU = 2.0000e+03     # [m/s]

```

```

    AI      = 1.3200e-45      # [s^3]
}

Kappa_aniso
{ * Lattice thermal conductivity
  * Formula = 0:
  * kappa() = 1 / ( 1/kappa + 1/kappa_b * T + 1/kappa_c * T^2 )
  * Formula = 1:
  * kappa() = kappa + kappa_b * T + kappa_c * T^2
  Formula = 1
    kappa   = 29      # [W/(K cm)]
}

* Investigating mechanical properties and thermal conductivity of 2D carbon-based materials by computational experiments
  kappa_b   = 0.0000e+00      # [W/(K^2 cm)]
  kappa_c   = 0.0000e+00      # [W/(K^3 cm)]

* AllDependent Thermal Conductivity
  wL_n      = 0.2      # [1]
  wL_p      = 0.02     # [1]
  wT_n      = 8        # [1]
  wT_p      = 6        # [1]
  wTU_n     = 9.0000e+05      # [1]
  wTU_p     = 2.0000e+06      # [1]
  b         = 1.8600e+02      # [1]
  M_n       = 30.9     # [Da]
  M_p       = 10.8     # [Da]
  R_n       = 1.2300e-10     # [m]
  R_p       = 1.1700e-10     # [m]
  r_del     = 1        # [1]
  Ax        = 0.0000e+00     # [s^3]
  eta       = 1.5000e-10     # [m]
  Eu_n      = 9        # [eV]
  Eu_p      = 45       # [eV]
  ED_n      = 1.33     # [eV]
  ED_p      = 1.33     # [eV]
  dLy       = 0.3      # [m]
  Lb        = 7.1600e-03     # [m]
  Q_n       = 4        # [1]
  Q_p       = 15       # [1]
  Nomg      = 3        # [1]
  order     = 2        # [1]
  epsilon   = 11.7     # [F/cm]
  m_c       = 0.9      # [kg]
  m_v       = 0.58     # [kg]
  rho       = 2.3290e+03     # [kg/m^3]
  BL        = 2.0000e-24     # [s/K^3]
  BT        = 9.3000e-13     # [1/K^4]
  BTU       = 5.5000e-18     # [s]
  omega1    = 2.3570e+13     # [1/s]
  omega2    = 2.7490e+13     # [1/s]
  omega3    = 7.4630e+13     # [1/s]
  omega4    = 4.5820e+13     # [1/s]
  M_h       = 28       # [Da]
  R_h       = 1.4600e-10     # [m]
  V_h       = 1.2100e-05     # [m^3/mol]
  vL        = 8.4800e+03     # [m/s]
  vLp       = 4.2400e+03     # [m/s]
  vT        = 5.8600e+03     # [m/s]
  vTU       = 2.0000e+03     # [m/s]
  AI        = 1.3200e-45     # [s^3]
}

Bandgap
{ * For conductors Band Gap is zero and the following parameters are used:
  * From Quantum ATK in metals WorkFunction and FermiEnergy are the same
    WorkFunction = 4.781765      # [eV]
    FermiEnergy  = 4.781765      # [eV]
  * for backward compatibility Chi0 could be used to define the work function.
}

eDOSMass
{
  * For effective mass specification Formula1 (me approximation):
  * or Formula2 (Nc300) can be used :
    Formula = 1      # [1]
}

```

```

* Formula1:
* me/m0 = [ (6 * mt)^2 * ml ]^(1/3) + mm
* mt = a[Eg(0)/Eg(T)]
* Nc(T) = 2(2pi*kB/h_Planck^2*me*T)^3/2 = 2.5094e19 ((me/m0)*(T/300))^3/2
      a      = 0.0000e+00    # [1]
      ml     = 0.0000e+00    # [1]
      mm     = 0.859    # [1]
* From Quantum ATK
}

SchroedingerParameters:
{ * For the hole masses for Schroedinger equation you can
  * use different formulas.
  * 0: use the isotropic density of states effective mass
  * 1: (for materials with Si-like hole band structure)
  * m(k)/m0=1/(A+-sqrt(B+C*(xy)^2+(yz)^2+(zx)^2))
  * where k=(x,y,z) is unit normal vector in reciprocal
  * space. '+' for light hole band, '-' for heavy hole band
  * 2: Heavy hole mass mh and light hole mass ml are
  * specified explicitly.
  * Use me as electron mass for free-carrier effect in
  * the refractive index model.
  * For electron masses, the following formula options exist:
  * 0: use the isotropic density of states effective mass
  * 1: (for materials with Si-like hole band structure)
  * use the a, ml, and mm parameters from eDOSMass.
  * Typically, this leads to anisotropy.
      formula = 0, 3    # [1]
  * Lifting of degeneracy of bulk valleys. The value for
  * electrons is added to the band edge for the subband
  * ladder of lower degeneracy if positive, and subtracted
  * from the band edge for the ladder of higher degeneracy
  * if negative. (that is, the value of the band edge is
  * always increased). For holes, the value is subtracted from
  * the band edge for the heavy hole band is positive,
  * add added tp that of the light hole band if
  * negative. The signs are such that the shift always
  * moves the band edges 'outward', away from midgap. The
  * gap itself is defined as the separation of the
  * unshifted band edges and remains unaffected.
      offset = 0.0000e+00, 0.0000e+00    # [eV]
  * Alternative to the specification of formula, offset,
  * and masses, you can make an arbitrary number of ladder
  * specification, 'eLadder(mz, mxy, deg, dE) and hLadder(...)'
  * Here, mz is the quantization mass, mxy an in-plane DOS mass,
  * deg the ladder degeneracy, and dE an shift of the band edge
  * for the ladder (non-negative; the shift is always outward,
  * away from midgap). When present, we solve the Schroedinger
  * equation separately for each ladder
  * Temperatures in rescaling of the mxy for eLadder and hLadder
      ShiftTemperature = 1.0000e+10, 1.0000e+10    # [K]
}

Resistivity
{ * Resist(T) = Resist0 * ( 1 + TempCoef * ( T - 273 ) + TempCoef2 * ( T - 273 )^2 )
  Resist0 = 0.2e-03 # [ohm*cm]
  * Resistivity signature of Graphene-Based Fiber-Reinforced Composite Subjected to Mechanical Loading
  TempCoef = 2.07e-03 # [1/K]
  * Thermal-Resistance Effect of Graphene at High Temperatures in Nanoelectomechanical Temperature Sensors
  TempCoef2 = 0.0000e+00 # [1/K^2]
}

Resistivity_aniso
{ * Resist(T) = Resist0 * ( 1 + TempCoef * ( T - 273 ) + TempCoef2 * ( T - 273 )^2 )
  Resist0 = 0.2e-03 # [ohm*cm]
  * Resistivity signature of Graphene-Based Fiber-Reinforced Composite Subjected to Mechanical Loading
  TempCoef = 2.07e-03 # [1/K]
  * Thermal-Resistance Effect of Graphene at High Temperatures in Nanoelectomechanical Temperature Sensors
  TempCoef2 = 0.0000e+00 # [1/K^2]
}

```

## ANNEX C: CODE 3 - SDEVICE\_DES.CMD

```

# The following input has been generated by automatic wizard
* Input template for MOSFET device simulation in Single device mode

Electrode {
-- Electrical Boundary Condition Section --
* Note that electrode names and their parameter values are conventional
* Consider to adjust them if necessary
  { name="top" Voltage=0.0 } *Resist=50. }
  { name="bottom" Voltage=0.0 } *Resist=50. }
}
File {
-- Inputs/Outputs Definition Section --
* Note that file names are swb name convention related
* Consider to change them according to actual ones
  Grid = "@tdr@" * device structure/grid/doping in tdr-format
  Doping = "@doping@" * uncomment if grid/doping in DF-ISE format
  Current = "@plot@" * output file to keep IV/CV curves
  Plot = "@tdrdat@" * output file to plot 2D/3D fields with Tecplot
  Output = "@log@" * output log file
  Parameter="@parameter@" * model/material parameter file. Uncomment if needed
}
Physics {
-- Physical Model and Other Physics Related Feature Activation --
* Note that the following syntax may not reflect your technology specifics
* Consider to adjust it if necessary
  AreaFactor = 10 * scaling factor for terminal currents/capacitances
  Temperature = 297. * equilibrium temperature [K]
  RecGenHeat * turns on recombination/generation heat term
  Mobility( * variety of mobility models is available (see the manual)
    PhuMob * activate the Philips mobility model
    HighFieldSaturation( * turns on dependency on HFS
      CarrierTempDrive * uses carrier temperature as a model driving force
    )
    Enormal * turns on dependency on a surface roughness scattering
  )
  EffectiveIntrinsicDensity(
    BandGapNarrowing( * variety of BGN models is available (see the manual)
      oldSlotboom * turns on BGN according to Slotboom model
    )
  )
  Recombination( * variety of recombination models is available (see the manual)
    SRH( * turns on SRH model
      DopingDep * turns on doping dependent SRH recombination
    )
    Auger * turns on Auger recombination
  )
  eThermionic HeteroInterface
  hThermionic HeteroInterface
}

* The following will account for the Schottky barrier transport at metal/semiconductor interface.
Physics (MaterialInterface="Silicon/Metal") { Schottky eRecVelocity=@Vree@ hRecVelocity=@Vrhh@
  Recombination ( SurfaceSRH )
  Charge (Conc=2.7e13)
  eThermionic
  hThermionic
}

Plot {
-- Fields Definition To Be Viewed In Tecplot --
* Most popular fields are specified
* For the full field list refer to the manual
*- Doping Profiles
  Doping DonorConcentration AcceptorConcentration
*- Charge, field, potential and potential energy
  SpaceCharge
  ElectricField/Vector Potential
  BandGap EffectiveBandGap BandGapNarrowing ElectronAffinity
  ConductionBandEnergy ValenceBandEnergy
}

```



```

*- Carrier Densities:
  EffectiveIntrinsicDensity IntrinsicDensity
  eDensity hDensity
  eQuasiFermiEnergy hQuasiFermiEnergy
*- Currents and current components:
  eGradQuasiFermi/Vector hGradQuasiFermi/Vector
  eMobility hMobility eVelocity hVelocity
  Current/Vector eCurrent/Vector hCurrent/Vector
  eDriftVelocity/Vector hDriftVelocity/Vector
*- SRH & interfacial traps
  SRHrecombination
  tSRHrecombination
*- Band2Band Tunneling & II
  eBand2BandGeneration hBand2BandGeneration Band2BandGeneration
  eAvalanche hAvalanche Avalanche
}

Math {
-- Parallelization on multi-CPU machine --
  Number_Of_Threads=1 * change the number of threads to > 1 to make parallelization possible.
                       * first make sure your machine has shared memory multi-CPU configuration.
                       * note that parallelization only works with ParDiSo and ILS linear solvers
-- Numerical/Solver Controls --
  Extrapolate          * turns on solution extrapolation along a bias ramp
  Derivatives          * considers mobility derivatives in Jacobian (recommended)
  Iterations=15        * maximum allowed number of Newton iterations (1D/2D)
  Digits=5             * relative error control value. Iterations are stopped if dx/x < 10^(-Digits)
  Method=ParDiSo       * use the direct linear solver (1D/2D)
  NotDamped=100        * number of Newton iterations over which the RHS-norm is allowed to increase
  Transient=BE         * turns on BE transient method
  ParallelToInterfaceInBoundaryLayer * mobility and avalanche driving force control along interfaces
  * CNormPrint         * uncomment to monitor a convergence behavior
)
}
Solve {
-- Section Which Contains Simulation Commands To Be Performed And Their Options--

*-- Solving the initial guess
  coupled (Iterations=100 LineSearchDamping=0.1) { Poisson }
  coupled (Iterations=100 LineSearchDamping=0.1) { Poisson Electron Hole }
  Quasistationary (
    InitialStep=1.e-1 MaxStep=0.1 Minstep=1.e-3 Increment=1.2
    Goal { Name=top Voltage=0.5 }
    plot { range=(0, 1) intervals=30 }
  )
  { Coupled { Poisson Electron Hole } }

*--Gate bias sweep. Consider the gate bias change if needed

  Quasistationary (
    InitialStep=1.e-3 MaxStep=0.04 Minstep=1.e-6 Increment=1.41
    Goal { Name=top Voltage=-0.5 }
    plot { range=(0, 1) intervals=100 }
  )
  { Coupled { Poisson Electron Hole }
    CurrentPlot(Time=(Range=(0 1) Intervals=100))
  }
}
}

```

## ANNEX D: CODE 4 - SDEVICE\_DES1.CMD

```

# The following input has been generated by automatic wizard
* Input template for MOSFET device simulation in Single device mode

Electrode {
-- Electrical Boundary Condition Section --
* Note that electrode names and their parameter values are conventional
* Consider to adjust them if necessary
  { name="top" Voltage=0.0 } *Resist=50. }
  { name="bottom" Voltage=0.0 } *Resist=50. }
}

File {
-- Inputs/Outputs Definition Section --
* Note that file names are swb name convention related
* Consider to change them according to actual ones
  Grid = "@tdr@" * device structure/grid/doping in tdr-format
* Doping = "@doping@" * uncomment if grid/doping in DF-ISE format
  Current = "@plot@" * output file to keep IV/CV curves
  Plot = "@tdrdat@" * output file to plot 2D/3D fields with Tecplot
  Output = "@log@" * output log file
  Parameter= "@parameter@" * model/material parameter file. Uncomment if needed
}

Physics {
-- Physical Model and Other Physics Related Feature Activation --
* Note that the following syntax may not reflect your technology specifics
* Consider to adjust it if necessary
  AreaFactor = 10 * scaling factor for terminal currents/capacitances
  Temperature = 297. * equilibrium temperature [K]
  RecGenHeat * turns on recombination/generation heat term
  Mobility( * variety of mobility models is available (see the manual)
    PhuMob * activate the Philips mobility model
    HighFieldSaturation( * turns on dependency on HFS
      CarrierTempDrive * uses carrier temperature as a model driving force
    )
  )
  Enormal * turns on dependency on a surface roughness scattering
)
EffectiveIntrinsicDensity(
  BandGapNarrowing( * variety of BGN models is available (see the manual)
    oldSlotboom * turns on BGN according to Slotboom model
  )
)
Recombination( * variety of recombination models is available (see the manual)
  SRH( * turns on SRH model
    DopingDep * turns on doping dependent SRH recombination
  )
  Auger * turns on Auger recombination
)
eThermionic HeteroInterface
hThermionic HeteroInterface
eBarrierTunneling "NLM" (Band2Band=Simple)
hBarrierTunneling "NLM" (Band2Band=Simple)
}

* The following will account for the Schottky barrier transport at metal/semiconductor interface.
Physics (MaterialInterface="Silicon/Metal") { Schottky eRecVelocity=@Vree@ hRecVelocity=@Vrh@
  Recombination ( SurfaceSRH )
  Charge (Conc=2.7e13)
  eThermionic
  hThermionic
}

Plot {
-- Fields Definition To Be Viewed In Tecplot --
* Most popular fields are specified
* For the full field list refer to the manual
  *- Doping Profiles
  Doping DonorConcentration AcceptorConcentration
  *- Charge, field, potential and potential energy
  SpaceCharge
  ElectricField/Vector Potential
}

```

```

BandGap EffectiveBandGap BandGapNarrowing ElectronAffinity
ConductionBandEnergy ValenceBandEnergy
*- Carrier Densities:
EffectiveIntrinsicDensity IntrinsicDensity
eDensity hDensity
eQuasiFermiEnergy hQuasiFermiEnergy
*- Currents and current components:
eGradQuasiFermi/Vector hGradQuasiFermi/Vector
eMobility hMobility eVelocity hVelocity
Current/Vector eCurrent/Vector hCurrent/Vector
eDriftVelocity/Vector hDriftVelocity/Vector
*- SRH & interfacial traps
SRHrecombination
tSRHrecombination
*- Band2Band Tunneling & II
eBand2BandGeneration hBand2BandGeneration Band2BandGeneration
eAvalanche hAvalanche Avalanche
eBarrierTunneling hBarrierTunneling
}

Math {
-- Parallelization on multi-CPU machine --
Number_Of_Threads=1 * change the number of threads to > 1 to make parallelization possible.
* first make sure your machine has shared memory multi-CPU configuration.
* note that parallelization only works with ParDiSo and ILS linear solvers
-- Numerical/Solver Controls --
Extrapolate * turns on solution extrapolation along a bias ramp
Derivatives * considers mobility derivatives in Jacobian (recommended)
Iterations=15 * maximum allowed number of Newton iterations (1D/2D)
Digits=5 * relative error control value. Iterations are stopped if dx/x < 10^(-Digits)
Method=ParDiSo * use the direct linear solver (1D/2D)
NotDamped=100 * number of Newton iterations over which the RHS-norm is allowed to increase
Transient=BE * turns on BE transient method
ParallelToInterfaceInBoundaryLayer * mobility and avalanche driving force control along interfaces
* CNormPrint * uncomment to monitor a convergence behavior
NonLocal "NLM" (
MaterialInterface="Silicon/Metal"
Length=@lengthmin@
-Transparent(Material="Metal")
)
}
Solve {
-- Section Which Contains Simulation Commands To Be Performed And Their Options--

*-- Solving the initial guess
coupled (Iterations=100 LineSearchDamping=0.1) { Poisson }
coupled (Iterations=100 LineSearchDamping=0.1) { Poisson Electron Hole }

Quasistationary (
InitialStep=1.e-1 MaxStep=0.1 Minstep=1.e-3 Increment=1.2
Goal { Name=top Voltage=0.5 }
plot { range=(0, 1) intervals=30 }
)
{ Coupled { Poisson Electron Hole } }

*--Gate bias sweep. Consider the gate bias change if needed

Quasistationary (
InitialStep=1.e-3 MaxStep=0.04 Minstep=1.e-6 Increment=1.41
Goal { Name=top Voltage=-0.5 }
plot { range=(0, 1) intervals=100 }
)
{ Coupled { Poisson Electron Hole }
CurrentPlot(Time=(Range=(0 1) Intervals=100))
}
}
}

```

**ANNEX E: CODE 5 - SDEVICE.PAR**

```
#define ParFileDir .  
  
Material="Metal" {  
  #includeext "ParFileDir/Metal.par"  
}  
  
Region="R.Doping" {  
  BarrierTunneling {  
    mt = 0.18, 0.18  
    g = 1, 1  
  }  
}
```